Multimodality Imaging for Epilepsy Diagnosis and Surgical Focus Localization: Three-Dimensional Image Correlation and Dual Isotope SPECT

Benjamin H. Brinkmann, Richard A. Robb, Terence J. O'Brien, Michael K. O'Connor, Brian P. Mullan
Biomedical Imaging Resource, Dept. of Neurology, and Dept. of Nuclear Medicine, Mayo Foundation, Rochester, MN 55905

Abstract

Peri-ictal SPECT is a potentially powerful tool to study changes in regional cerebral blood flow during a partial seizure and to localize the seizure focus for pre-surgical evaluation. Recently we have developed and validated a method for co-registering and normalizing 3D interictal SPECT images to 3D ictal SPECT images and deriving a difference image co-registered to the patient's 3D MRI. This method has been shown to significantly improve clinical outcomes in surgery patients. In order to improve the method's sensitivity and specificity a number of enhancements have been added to the basic technique, including using voxel-based registration to better align ictal and interictal images, dual isotope (Tc-99m and I-123) SPECT for effective tissue discrimination, and a custom software interface written to facilitate the entire process. We report results that show significant improvement over the original method, and we discuss future work which should continue to improve the method as a clinical tool.

Introduction

Localizing the epileptogenic zone, or seizure focus, in partial epilepsy is a challenging clinical problem. Currently 20-50% of intractable partial epilepsy cases are unlocalized by conventional methods, which include scalp-recorded electroencephalography (EEG), magnetic resonance imaging (MRI), and side-by-side visual analysis of peri-ictal (during or immediately after the seizure) and interictal (baseline, non-seizure) single photon emission computed tomography (SPECT) images. EEG gives functional information with high temporal resolution, but provides only vague anatomical seizure localization. MRI gives excellent soft tissue contrast but fails to identify the epileptogenic zone in the absence of an obvious structural lesion. Intracranial EEG is generally reserved for only the most difficult cases because of its invasiveness and potential for morbidity. Positron emission tomography (PET) may also be used, but is not available to most epilepsy centers due to its high cost and the difficulty of obtaining positron emitting isotopes.

Subtraction ictal SPECT coregistered to MRI (SISCOM) [1] is a recent advance in the field of peri-ictal functional imaging and has been shown to significantly improve surgical outcomes in epilepsy patients [2]. Several groups have simultaneously developed comparable methodologies for studying regional cerebral blood flow (rCBF) during and after epileptic seizures [3-5]. The SISCOM technique involves the intravenous injection during a partial seizure (ictal SPECT) or immediately following one (post-ictal SPECT) of a radiotracer exhibiting a high first pass cerebral extraction rate and a low back diffusion. Radiotracers with these properties include Tc-99m hexamethylpropylene amine oxime (HMPAO), Tc-99m ethyl cysteinate diethylester (ECD) and I-123 iodoamphetamine (IMP). The SPECT images can be acquired up to several hours following the event, providing a semi-quantitative image of the rCBF present between 30 and 120 seconds after the injection [6, 7]. A second SPECT image is acquired at a later time under resting conditions (interictal SPECT) to serve as a baseline image. The peri-ictal and interictal images are co-registered, normalized, subtracted, and thresholded to produce an image representing focal activation sites during the seizure. This image is then registered to the patient's MRI and displayed to provide an anatomical context for the func-

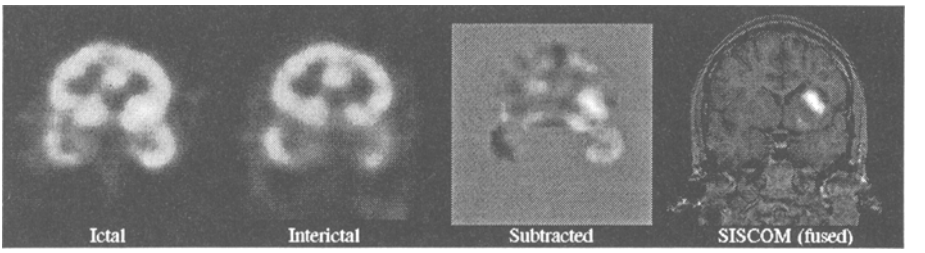

Figure 1A: SISCOM and its component images: ictal SPECT, registered interictal SPECT, subtraction (ictal-interictal) SPECT, and the thresholded subtraction image fused with the patient's MRI. The SISCOM image shows a clear right insular focal activation site. Ictal-interictal registration was performed with AIR, while surface matching was used for SPECT-MRI registration.

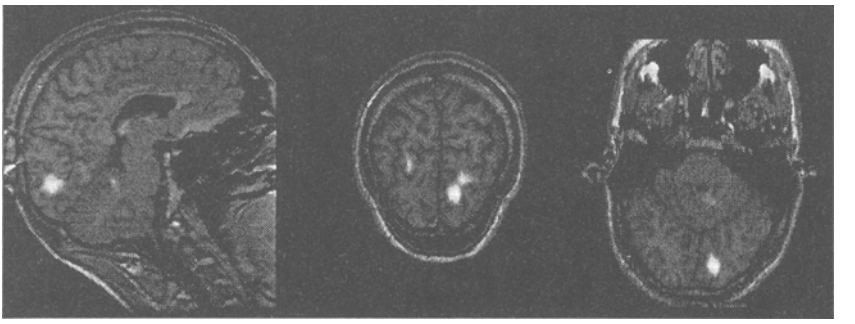

Figure 1B: SISCOM images allow three-dimensional perspectives on the anatomic context of the functional activation site and can be viewed in sagittal (left), coronal (middle), transverse (right), or oblique orientations.

tional activation sites. Figure 1 illustrates the SISCOM image and its component images, as well as its capacity for providing three-dimensional functional and anatomical information.

While conventional SISCOM is a powerful tool for studying neuroactivation in partial epilepsy, it has a number of limitations which advanced image processing and analysis techniques can improve. One important limitation is that while seizures are dynamic phenomena, SPECT is only able to give a single snapshot of the blood flow pattern during a limited time window of the seizure. It is therefore very difficult with current SPECT methods to study the evolution of blood flow changes occurring during and after an epileptic seizure. Another limitation arises from small inaccuracies in the interictal to peri-ictal registration, which can significantly degrade focal spot intensity, accuracy, and detectability [8]. A further limitation of the method is the processing time required for producing the SISCOM images, which can easily approach an hour for an experienced physician. To date at our institution we have evaluated over three hundred forty epilepsy patients using the SISCOM method, which has created a significant time burden on clinicians and residents.

To address these limitations, we have undertaken a number of studies directed at improving the accuracy, reliability, and speed of the SISCOM technique. This paper reports the development and validation of several enhancements to the basic SISCOM method. These developments include voxel-based registration to align the peri-ictal and interictal SPECT images, dual-isotope I-123 and Tc-99m SPECT to provide multiple rCBF maps during a single seizure, and customized software to reduce operator time requirements. We also present several additional improvements we plan to implement in the near future.

Voxel-based SPECT Registration

One of the major factors in the quality and diagnostic utility of the SPECT subtraction image is the accuracy of interictal and peri-ictal SPECT image co-registration. It has been shown that even small misregistrations may reduce the focal spot intensity significantly in paired functional activation images [8]. The original SISCOM method uses surface matching co-registration [10] and consistently matches images with better than 1 voxel dimension of accuracy [1], but it is desirable to extend this accuracy as much as possible to improve the sensitivity and specificity of epileptogenic localization. Voxel-based registration methods have been shown to be more accurate than surface matching methods at a variety of coregistration tasks [11]. However, few have been quantitatively compared for functional SPECT rCBF images, and the performance of different algorithms depends greatly on the registration task to be performed. It has been unclear whether the large changes in image contrast that accompany ictal activation could confound voxel-based registration.

An approach to image matching by maximization of mutual information was described by Wells [12] in 1996. The implementation we used is available in the AnalyzeAVW software package [9] and uses the simplex method to maximize the mutual information of the two images. In contrast, the well-known AIR (or Woods') algorithm [14,15] aligns two images by first thresholding to remove background noise and then using a Newton-Raphson method to minimize the standard deviation of the ratio of corresponding image gray values. We conducted experiments to examine and compare surface matching, mutual information, and AIR registration algorithms and provide a quantitative estimate of their accuracy for aligning peri-ictal and interictal patient SPECT images.

Methods

For surface matching, binary images were created by thresholding. Ventricle and other interior holes were filled using two-dimensional math morphology [9]. Matches were performed with one thousand sample points on the match volume surface. For the mutual information algorithm, default parameters were used (parameter tolerance 1x10-8, function tolerance 0.001, 1000 iterations per step) with the exception of the subsampling parameters, which were found to give superior results with 1:1 sampling for all steps. For Woods' algorithm we used AIR 3.0, obtained from the author. The default convergence change threshold (0.00001) was used, as was the default sampling (81:1 with a factor of 3 decrement at each step) as this sampling approach was found to give better results than the 1:1 sampling used with mutual information. The same intensity thresholds were used for the AIR algorithm as were used in the surface matching algorithm. No smoothing kernel was used. Computation time was not formally considered in this study.

Image	X Rot	Y Rot	Z Rot	Z Trans
1	0.0	0.0	0.0	0.0
2	-14.9	-14.9	1.5	-2.5
3	-10.0	-10.0	3.0	-2.0
4	-5.0	-5.0	5.0	-1.5
5	-3.0	-3.0	10.0	-1.0
6	-1.5	-1.5	14.9	-0.5

Table 1: Misregistrations applied to the brain phantom and patient simulation images. Rotations are given in degrees, while translations are given in voxel units.

Six sequential scans of a realistic 3D volumetric brain phantom (Hoffman 3D brain phantom, Data Spectrum Corp., Hillsborough, NC) containing 15 mCi of Tc-99m were taken, with rotations applied about the central axis of the scanner to the phantom in a headrest. A digital spirit level (Pro Smart Level, Wedge Innovations, San Jose, CA) was used to measure rotation angles, and images were acquired at 0.0, 1.5, 3.0, 5.0, 10.0, and 14.9 degrees. The images were reconstructed on a 64x64 grid with cubic voxel dimensions of 4.4 mm per side using a third-order Metz filter (6mm FWHM). To provide a more challenging registration task using four degrees of freedom, the reconstructed images were then misaligned by known X and Y rotations and Z translations (Table 1) using the AnalyzeAVW software system [9]. Each scan was then registered to the other five, creating fifteen registration tasks to be evaluated for each of the three algorithms. Reference 4x4 transformation matrices were constructed using the known rotation and translation parameters, and these matrices were inverted and multiplied by the matrices given by the registration algorithms, producing residual error matrices. These matrices were evaluated to find the distance in millimeters by which a point on the cortical surface would be misaligned relative to its true position, at the maximum measured radius on the phantom's surface of 79.3 mm.

The phantom images approximate patient SPECT scans with very little functional rCBF change. To approximate a patient SPECT with severe ("worst case") rCBF changes, we obtained a true ictal patient image (patient #2 below) and manually replaced apparent focal activation sites with the mean cerebral pixel intensity. We then systematically modified the contrast in various parts of the image by adding areas of increased and decreased rCBF (bright and dark pixels, respectively). The image was blurred in the transverse plane with a 3x3 mean filter, and zero-mean Gaussian noise (18% of mean cerebral pixel count) was added. The resulting image had very different contrast (and hence rCBF patterns) and reduced resolution compared to the patient's ictal image, but had identical shape and was in perfect coregistration to it. The registration experiment used with the phantom was repeated using the ictal and simulated patient images. The rotations and translations listed in Table 1 were applied to both the ictal and simulated images and the fifteen matching tasks were performed using the ictal image as the base volume and the simulated image as the match volume in each experiment.

Interictal and peri-ictal Tc-99m SPECT images were obtained from fifteen sequentially enrolled epilepsy patients. Informed consent was obtained. Each patient's interictal scan was matched to the corresponding ictal or post-ictal image using each of the three registration algorithms. A SISCOM subtraction image was created for each image pair, and the standard deviation of non-zero pixels in this image was recorded for each of the registration algorithms. This value is comparable to the root mean squared difference between the two images, and would be expected to be small when the images are well registered [16].

Results and Discussion: Registration

Registration results for the six brain phantom SPECT images and for the simulation image are shown in Table 2. For the phantom data the voxel-based methods showed a statistically significant improvement over the surface-based method with $p<0.0005$ (analysis of variance (ANOVA) for repeated measures), while there were no significant differences between mutual information and the AIR algorithm (ANOVA for planned comparisons). For the simulation experiment, the voxel-based methods were significantly better than surface matching with $p<0.0001$ (ANOVA for repeated measures) and AIR showed a statistically significant improvement over mutual information with $p<0.05$ (ANOVA for planned comparisons).

The fifteen patient peri-ictal and interictal SPECT subtraction images had standard deviations of 12.18±1.16, 11.38±1.33, and 10.98±1.24 (mean ± st.dev.) for surface matching, mutual information, and the AIR algorithm, respectively. The improvement in patient standard deviation data for voxel matching over surface matching is statistically significant with $p<0.0001$ (ANOVA for repeated measures), and AIR's results show sta-

	Phantom		Simulation	
	Mean±St.Dev	Range	Mean±St.Dev	Range
Surface Matching	3.08±1.16	1.09-4.47	2.49±1.22	0.30-4.54
Mutual Information	1.84±0.68	0.70-3.20	0.88±0.81	0.03-2.57
AIR 3.0	1.98±1.01	0.77-4.95	0.54±0.40	0.22-1.77

Table 2: Mean, standard deviation, and range results from the phantom and patient simulation registration experiments. All values are given as total error in millimeters.

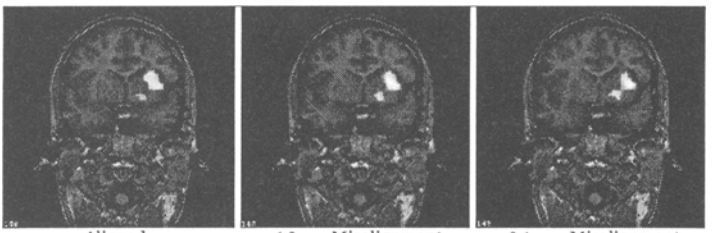

Figure 2: The effects of misregistration on SISCOM images. As the ictal and interictal SPECT images are misaligned, the intensity of the focal spot decreases and its shape changes.

tistically significant improvement over mutual information with $p<0.05$ (ANOVA for planned comparisons).

Figure 2 illustrates the importance of accuracy in the ictal-interictal SPECT coregistration. With even small misregistrations the apparent intensity and position of the focal activation spot may change. The superiority of voxel-based methods over surface matching corresponds with findings in the current literature [11] and suggests that in spite of the rCBF differences between ictal and interictal SPECT images, voxel intensity based measures are still more reliable than the cortical surface shape for registration, particularly in low-resolution SPECT images. This data also highlights the differences between mutual information and AIR. The phantom results (no rCBF changes) show a statistically insignificant trend in favor of mutual information, suggesting that further study might show it to be more accurate than AIR for static contrast images. However, AIR is more robust to the ictal-interictal rCBF changes than mutual information, although further study is necessary to determine whether this statistically significant result is clinically significant. The mutual information cost function tends to align images such that voxel intensity values in one image are maximally predictive of intensity values in the other, which does not necessarily hold with large rCBF changes. AIR tends to reduce variation in the ratio image, which is dominated by contributions from misregistration around sharp intensity transitions, such as the ventricles and image edges.

Dual-Isotope SPECT

A dual-isotope, double-injection technique using sequential injections of two radiopharmaceuticals with different energy photopeaks would provide a number of advantages to the SISCOM method by producing two different simultaneously-acquired rCBF images. First, such a method could be used to document the changes occurring over time during a single seizure. As both Tc-99m-ECD and I-123-IMP show similar brain uptake kinetics that closely reflect the pattern of cerebral blood flow shortly after their injection [17-22], the differences between the images should reflect changes in rCBF between the injections. Second, the dual isotope method would allow the subtraction of a post-ictal image from a simultaneously-acquired and perfectly coregistered ictal image. This completely eliminates misregistration noise from the SISCOM subtraction image and furthermore avoids the inconvenience and expense to the patient of returning to the institution for a separate interictal SPECT. In addition, the magnitude of

the focal hypoperfusion in the post-ictal seizure focus is believed to be greater and more reliable than interictal epileptogenic hypoperfusion [23-26]. As a result, the magnitude of the focal difference in the subtraction images in the region of the epileptogenic zone should be greater by subtracting from the ictal SPECT a post-ictal SPECT rather than an interictal SPECT.

The purpose of these experiments is to develop and validate an accurate method for performing dual isotope Tc-99m ECD and I-123 IMP SPECT imaging in epilepsy patients. Previous authors have attempted dual isotope SPECT for studying cerebral ischemia [27,28], cerebrovascular interventions [29], and ratio images for cognitive activation studies [30,31]. In quantitative SPECT studies of epilepsy patients the accuracy of rCBF maps, in particular the absence of isotope crosstalk, is crucial, and we have found previous methods [27-32], which have used asymmetric I-123 energy windows offset by varying amounts, inadequate for these purposes.

Methods

A Hoffman brain slice phantom (Data Spectrum Corp., Chapel Hill, NC) was used, which consisted of two flat layers with seven independent fluid compartments simulating realistic cortex and white matter areas in a two-dimensional transaxial slice through the lentiform nucleus and corpus collosum (Figure 3). Six of the compartments were relatively small and were located in the left half of the top layer of the phantom. The seventh compartment was large, spanning the entire bottom layer of the phantom and protruding through to the top layer in the right hemisphere of the phantom (Figure 3A). Compartments 1-4 (total volume 18.6 ml) in the anterior left of the phantom were designated I-123 only compartments, whereas compartments 5 and 6 (total volume 12.3 ml) in the posterior left of the phantom were designated Tc-99m only compartments. The large compartment, No. 7 (96.3 ml), was designated for mixed isotopes. The phantom's perimeter was surrounded by a layer of simulated bone to replicate bone scatter in tomographic acquisitions.

Planar images of the brain phantom were taken with one head of a dual-headed gamma camera system (Helix, Elscint Inc., Haifa, Israel) and were used to develop the dual isotope acquisition technique. Acquisitions were performed using a high resolution parallel hole collimator, obtaining 32 energy band images 2 keV in width, from 120 keV to 184 keV. Intensity parameters were measured using regions of interest in AnalyzeAVW [9] on each of the 2 keV band images. The ROI areas measured are shown in Figure 3: Tc-99m only (T), I-123 only (I), both isotope (B), white matter or cerebral background (BG), and extracerebral background areas (A). These parameters were then plotted across the 32 energy bands and were used to determine the best combination of energy window settings for the Tc-99m and I-123 images. Figure 3A illustrates that it is

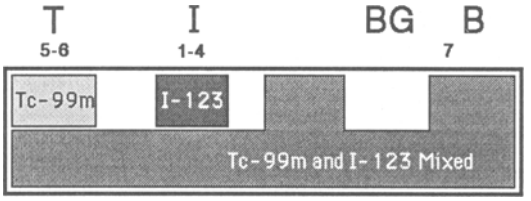

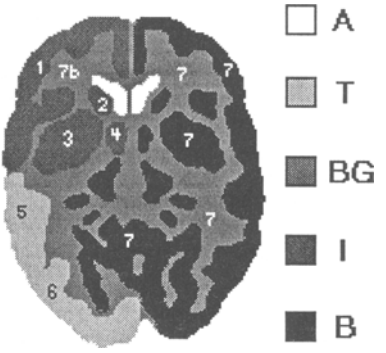

Figure 3: A) A simulated cross section through the Hoffman brain slice phantom. Labels and chamber numbers correspond to those shown in Figure 3B. **B)** A planar diagram of the Hoffman brain slice phantom. Areas are mixed isotopes (B), I-123 (I), bottom layer mixed isotopes (BG), Tc-99m (T), and air or isotope-free areas (A).

necessary to subtract the BG signal from the T and I signals to isolate the Tc-99m and I-123 signals from the large, underlying mixed-isotope compartment. Hence, signal above baseline (SAB)

$$SAB_I = I - BG \qquad SAB_{Tc} = T - BG$$

represents the signal in the single isotope compartments, while percent crosstalk (PC)

$$PC_I = \frac{SAB_{Tc}}{SAB_I} \qquad PC_{Tc} = \frac{SAB_I}{SAB_{Tc}}$$

represents crosstalk from the opposing isotope as a percentage of each isotope's signal.

Energy bands were added together using AnalyzeAVW and specialized software written in Tcl/Tk with the AVW image processing libraries. The energy band images were summed to create images with different energy window settings, allowing us to replicate and compare results from the literature [27-32] to within 1 keV. Optimal settings were chosen based upon SAB and PC, as well as signal to noise ratio (SNR), defined as the isotope SAB divided by the extracerebral background signal. The dual-isotope images were compared to reference Tc-99m only (130-146 keV, phantom containing no I-123) and I-123 only (152-168 keV, phantom containing no Tc-99m) images for validation.

Crosstalk from Tc-99m represents a significant problem in the relatively count-poor I-123 image. To compensate for this, a 4% asymmetric window (134-140 keV) was used to isolate the Tc-99m signal from I-123 contamination and septal penetration, and this then provided a spatial map for subtracting the Tc-99m crosstalk from the I-123 window. The contamination correction fraction was calculated by filling the phantom with Tc-99m only, measuring the counts in the Tc-99m compartment of the phantom across the energy spectrum, and dividing the counts in each energy band by the number of counts in the same ROI in the 4% photopeak image (Table 3). Correction values less than 0.0005 were observed to consist primarily of background noise and were therefore set to zero. The total correction factor for a given energy window is obtained by summing the energy band correction factors over the energy range used.

Tomographic images of the phantom containing I-123 only, Tc-99m only, and a 3:1 Tc:I mixture were acquired using a high-resolution fan beam collimator with the energy windows set according to the arrangement determined with the planar data. Image data was reconstructed using a standard filtered-back-projection algorithm in word mode

Energy Band	Correction Factor
144-146	0.2417
146-148	0.1518
148-150	0.09572
150-152	0.04291
152-154	0.02575
154-156	0.008773
156-158	0.003661
158-160	0.001707
160-162	0.0008535

Table 3: Correction factors for Tc-99m crosstalk in the energy windows used to construct the I-123. Correction factors above 162 keV were negligible.

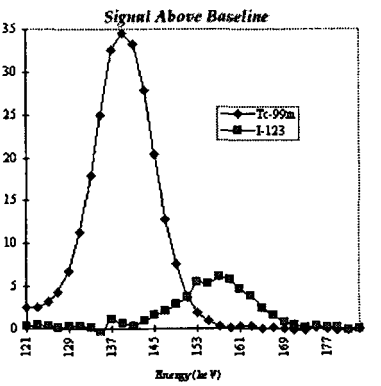

Figure 4: Signal above baseline plotted against gamma ray energy.

	Brinkmann		Asymm. I-123 [29-31]		Shifted I-123 [27,28,32]	
	Tc-99m	I-123	Tc-99m	I-123	Tc-99m	I-123
Window (keV)	130-146	152-168*	133-147	153-169	133-147	159-175
PC	2.79%	1.33%	3.60%	19.68%	3.60%	3.65%
SNR	180.10	14.73	185.67	15.25	185.67	7.98

*Subtractive crosstalk correction was applied

Table 4: Comparison of the reported dual isotope acquisition method with previously-reported methods in percent crosstalk (PC) and signal to noise ratio (SNR).

with a third-order Metz smoothing filter (6mm FWHM). No attenuation correction has been used to this point, but we expect that some attenuation correction may be useful for the Tc-99m image. The Tc-99m-only and I-123-only images were created with simple energy windows (130-146 keV and 152-168 keV, respectively) as references. The dual isotope images were compared to the reference I-123 and Tc-99m images using ROI intensity ratios. To estimate isotope crosstalk, the ratio of the opposite isotope compartment to the mixed isotope compartment (T/B for the I-123 image, and I/B for the Tc-99m image) was calculated for each dual isotope image, and these ratios were compared to the corresponding ratios for the reference single-isotope images.

Results and Discussion: Dual Isotope

Figure 4 plots the signal above baseline for Tc-99m and I-123 across the acquired energy spectrum. It illustrates that the Tc-99m and I-123 signals show significant overlap and crosstalk between 145 and 155 keV. For the Tc-99m image we used a 12% (130-146 keV) asymmetric window which maximized the Tc-99m counts in the image while minimizing I-123 crosstalk. The optimum I-123 image was obtained using an energy window of 152-168 keV (10%) with crosstalk correction by subtracting 0.041 of the Tc-99m correction image (134-140 keV) from the I-123 image. Figure 5 illustrates planar images formed from a portion of the overlap region (145-155keV), as well as the I-123 (center) and Tc-99m (right) dual isotope images formed using these methods.

Table 4 compares our planar dual isotope images to images created by replicating previously-reported methods [27-32] to within 1 keV in terms of PC and SNR. The Tc-99m images are all fairly comparable, with our strategy reducing counts slightly in favor of minimizing crosstalk. The I-123 image is the challenging part of the dual isotope strategy. Our reported acquisition shows a great deal less crosstalk than other methods and, in fact, offers nearly a tenfold reduction over most other methods [27-31]. Some methods [27,28,32] have reduced crosstalk by excluding nearly half the I-123 photopeak, reducing the SNR commensurately.

Crosstalk correction for the I-123 image was applied before and after image recon-

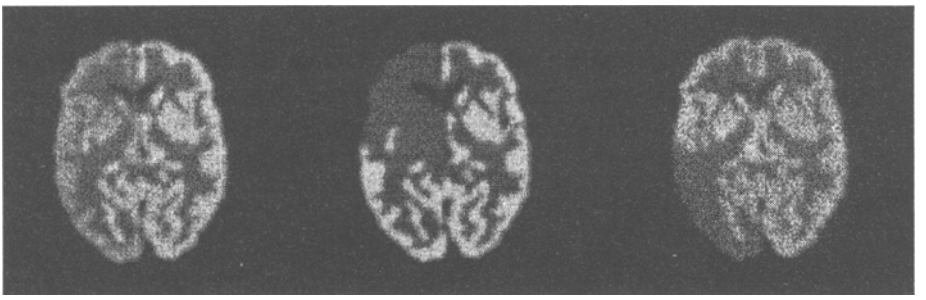

Figure 5: Planar images showing equal amounts of Tc-99m and I-123 signal (left) and the Tc-99m (center) and I-123 (right) dual isotope images using the reported acquisition strategy.

struction with essentially identical results. Post-reconstruction crosstalk correction is preferred for its practical ease and lower computation time. The tomographic dual isotope Tc-99m and I-123 images are shown in Figure 6. The reference I-123 image had a ratio of 0.3155, while the crosstalk-corrected dual isotope image had a ratio of 0.3202, i.e. a difference of 1.51%. A dual isotope I-123 image acquired using a simple energy window (152-168 keV) and no crosstalk correction had a ratio of 0.3547, a difference of 12.44% from the reference I-123 image. The dual isotope Tc-99m image had a ratio of 0.2657 compared to the reference Tc-99m image ratio of 0.2759, a difference of 3.70%. The dual isotope tomographic images differ only slightly from their single-isotope reference counterparts (and are visually indistinguishable), which suggests that accurate quantitative rCBF studies of epileptic seizures may be performed with this technique.

Customized Software

To alleviate the time requirements associated with performing SISCOM using a comprehensive general image analysis software package, a specialized software tool was created. This tool performs the SPECT processing, co-registration, subtraction, and analysis portion of SISCOM. The program has a graphical user interface that is simple and easy to use, and it places tools for the interactive portions of the SPECT image processing within easy reach while automating a large portion of the processing. The software was written in Tcl/Tk with the AVW image processing function libraries [13]. Tcl/Tk allows fast and simple graphical user interface design with a great deal of configurability, while the AVW library contains optimized imaging functions compiled in C. These imaging functions are called by the Tcl/Tk interpreter, providing fast execution. A synopsis of the program flow is as follows:

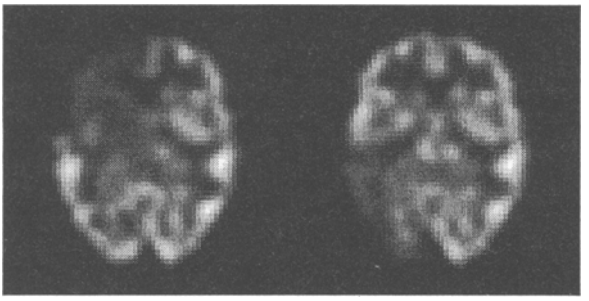

Figure 6: The tomographic dual isotope Tc-99m (left) and I-123 (right) images acquired using the reported method.

1. Interactively load ictal and interictal SPECT images
2. Interactively threshold images leaving only the cortical mantle
3. Use chosen thresholds and 2D (transaxial) morphology to create binary images with interior spaces filled
4. Register interictal SPECT to ictal SPECT using surface matching, mutual information, or Woods' AIR algorithm
5. Display registered images with linked cursors to allow the user to visually assess the success of the registration (see Figure 7)
6. Mask the ictal and registered interictal SPECT volumes using their respective binary images
7. Normalize ictal and registered interictal SPECT images to mean cerebral pixel intensity of 100 (for 8-bit images)
8. Subtract interictal SPECT from ictal SPECT
9. Calculate the standard deviation of the nonzero pixels in the subtraction image
10. Threshold the subtraction image at two standard deviations to identify significant activation sites
11. Display final and intermediate images for review

This can take under two minutes for an experienced user on a Silicon Graphics Indy workstation, compared with around 40 minutes for the same tasks using generalized software. Most of this time is spent switching between programs, saving intermediate image volumes to disk, and performing tasks which are easily automated. It is not possible at this time to train technicians to perform these functions, as the physician must screen the procedure for errors, including misregistration, left-right image transposition, and image artifacts or inaccurate header (voxel size, image orientation, etc.) information. The MRI coregistration portion of SISCOM is in the process of being added to the customized software.

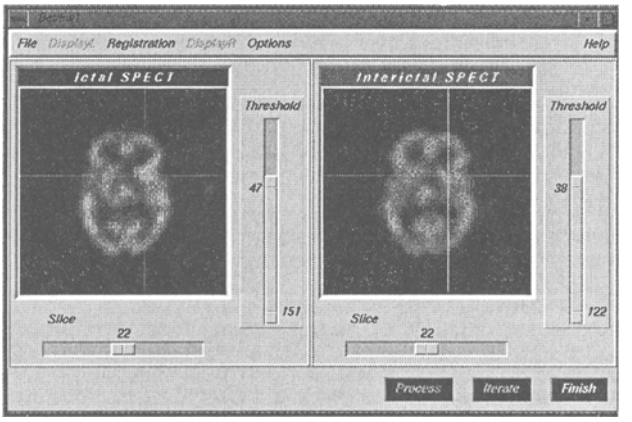

Figure 7: A screen shot from the customized SISCOM software program. Registration accuracy is visually assessed using the linked cursor tool shown.

Future Work

In a previous study [33] we described and validated a method for coregistering scalp EEG electrode positions to a patient's volumetric MRI. Subsequently we have begun using this procedure on epilepsy patients and have improved our methods for EEG topographic mapping. The next step in extending the diagnostic power of SISCOM is to add scalp-recorded EEG topographic maps and neural source dipole estimates to SISCOM, creating a more comprehensive picture of neurological activity during an epileptic seizure.

Conclusions

We have developed and evaluated imaging methods which have improved diagnostic accuracy and speed for a clinically-useful [2] method which is currently being used to evaluate epilepsy patients at our institution. First, voxel-based registration algorithms have been shown to significantly improve the accuracy of registering patient peri-ictal and interictal SPECT scans, which should increase the diagnostic capability of SISCOM. Second, the dual-isotope double-injection method allows dynamic studies of seizure propagation patterns and demonstrates promise for enhancing SISCOM's sensitivity by taking advantage of post-ictal epileptogenic hypoperfusion and by eliminating misregistration noise. Third, the development of customized software has allowed more epilepsy patients to benefit from the SISCOM methodology and has reduced the time requirements on physicians for image processing and analysis. The synergistic effect of these advances is to provide a more comprehensive picture of epileptic neurophysiology and to improve the capacity of physicians to effectively diagnose and treat focal epilepsy.

References

1. O'Brien TJ, O'Connor MK, Mullan BP, Brinkmann BH, Hanson DP, Jack CR, So EL. Seduction ictal SPECT co-registered to MRI in partial epilepsy: Description and technical validation of the method with phantom and patient studies. *Nuc Med Comm* 1998;19:31-45.
2. O'Brien TJ, So EL, Mullan BP, et al. Subtraction Ictal SPECT Co-Registered To MRI Improves Clinical Usefulness Of SPECT In Localizing The Surgical Seizure Focus. *Neurology* 1998;50:445-454.

3. Zubal IG, Spencer SS, Imam K, Smith EO, Wisniewski G, Hoffer PB. Difference images calculated from ictal and interictal technetium-99m-HMPAO SPECT scans of epilepsy. *J Nuc Med* 1995;36:684-689.
4. Weder B, Oettli R, Maguire RP, Vonesch T. Partial epileptic seizure with versive movements examined by [99mTc]HM-PAO brain single photon emission computed tomography: An early postictal case study analyzed by computerized brain atlas methods. *Epilepsia* 1996;37:68-75.
5. Chiron C, Jaminska A, Cieuta C, Vera P, Plouin P, Dulac O. Ictal and interictal subtraction ECD-SPECT in refectory childhood epilepsy. *Epilepsia* 1997;38 (Suppl. 3):9.
6. Berkovic SF, Newton M, Chiron C, Dulac O. Single photon emission tomography. In: Engel J Jr, ed. *Surgical treatment of the epilepsies*. New York: Raven Press, 1993:233-243.
7. Mullan BP, O'Connor M, Hung J. Single photon emission computed tomography. *Neuroimaging Clinics of North America* 1995;5:647-673.
8. Sychra JJ, Pavel DG, Chen Y, and Jani A. The accuracy of SPECT brain activation images: Propagation of registration errors. *Medical Physics* 1994. 21(12):1927-32.
9. Hanson DP, Robb RA, Aharon S, Augustine KE, Cameron BM, Camp JJ, Karwoski RA, Larson AG, Stacy MC, Workman EL. New software toolkits for comprehensive visualization and analysis of three-dimensional multimodal biomedical images. *J Digital Imaging* 1997. 10(2)(Suppl. 1-August):31-35.
10. Jiang, H., Robb, R. A., and Holton K. S. "A new approach to 3-D registration of multimodality medical images by surface matching." *Proc VBC '92,* 1992. Vol. 1808, pp. 196-213.
11. West, J., Fitzpatrick, J.M., Wang, M.Y., et. al. Comparison and evaluation of retrospective intermodality brain image registration techniques. *Journal of Computer Assisted Tomography,* 1997, 21(4):554-566.
12. Wells, W. M. III, Viola, P., Atsumi, H., Nakajima, S., and Kikinis, R. Mulit-modal volume registration by maximization of mutual information. *Medical Image Analysis*, 1996. 1(1):35-51.
13. Robb RA, Aharon S, Augustine KE, Cameron BM, Camp JJ, Hanson, DP, Karwoski RA, Larson AG, Stacy MC, Workman EL. *AVW Reference Manual* Technical Report, 1997.
14. Woods, R.P., Cherry, S.R., and Mazziotta, J.C. Rapid automated algorithm for aligning and reslicing PET images. *J Comp Asst Tomo*, 1992. 14(4):620-633.
15. Woods RP, Mazziotta JC, Cherry SR. MRI-PET registration with automated algorithm. *J Comp Asst Tomo* 1993. 17:536-46.
16. Lange N. Some computational and statistical tools for paired comparisons of digital images. *Stat Meth Med Res* 1994. 3:23-40.
17. Greenberg JH, Araki N, Karp A, et al. Quantitative measurement of regional cerebral blood flow in focal cerebral ischemia using Tc-99m-ECD. (Abstract). *J Nucl Med* 1991;32:1070.
18. Devous MD, Payne JK, Lowe JL, Leroy RF. Comparisons of 99mTc-EDC to 133Xe SPECT in normal controls and in patients with mild-moderate regional cerebral blood flow abnormalities. *J Nucl Med* 1993;34:754-761.
19. Kuhl D, Barrco J, Huang S, et al. Quantifying local cerebral blood flow with N-isopropyl-p-I-123 iodoamphetamine (IMP) tomography. *J Nucl Med* 1982;23:196-203.
20. Takeshita G, Maeda H, Nakane K, et al. Quantitaive measurement of regional perfusion using N-isopropyl-(iodine-123)p-iodoamphetamine and single photon emission computed tomography. *J Nucl Med* 1992;33:1741-1749.
21. Greenberg JH, Kushner M, Rangi M, et al. Validation studies of iodine-123 iodoamphetamine as a cerebral blood flow tracer using emission tomography. *J Nucl Med* 1990;31:1364-1369.
22. Matsuda H SH, Sumiya H, et al. Quantifying local cerebral blood flow by N-isopropyl-(iodine-123)p-iodoamphetamine and single photon emission computed tomography with rotating gamma camera. *Am J Physiol Imaging* 1986;1:186-194.6.
23. Newton MR, Berkovic SF, Austin MC, Rowe CC, McKay WJ, Bladin PF. Postictal switch in blood flow distribution and temporal lobe seizures. *J Neurol Neurosurg Psychiatry* 1992;55:891-894.
24. Newton MR, Berkovic S, Austin M, Rowe C, McKay W, Bladin P. Ictal postictal and interictal single-photon emission tomography in the lateralization of temporal lobe epilepsy. *Eur J Nuc Med* 1994;21:1067-1071.
25. Rowe CC, Berkovic SF, Austin MC, McKay WJ, Bladin PF. Patterns of postictal cerebral blood flow in temporal lobe epilepsy: Quanlitative and quantitative analysis. *Neurology* 1991;41:1096-1103.
26. Rowe CC, Berkovic SF, Sia STB, Austin M, McKay WJ, Kalnins RM, Bladdin PF. Localization of epileptic foci with postictal single photon emission computed tomography. *Ann Neurol* 1989;26:660-668.

27. Devous MD Sr., Lowe JL, Payne JK. Dual-isotope brain SPECT imaging with Technetium-99m and Iodine-123: Clinical validation using Xenon-133 SPECT. *J Nucl Med* 1992. 33(11): 1919-24.
28. Devous MD Sr., Lowe JL, Payne JK. Dual-isotope brain SPECT imaging with Technetium-99m and Iodine-123: Validation by phantom studies. *J Nucl Med 1992*. 33(11): 2030-35.
29. Mathews D, Walker BS, Allen BC, Batjer H, Purdy PD. Diagnostic applications of simultaneously acquired dual-isotope single-photon emission CT scans. *AJNR* 1994. 15:63-71.
30. Madsen MT, O'Leary DS, Andreasen NC, Kirchner PT. Dual isotope brain SPECT imaging for monitoring cognitive activation: Physical considerations. *Nuc Med Comm* 1993. 14:391-6.
31. O'Leary DS, Madsen MT, Hurtig R, Kirchner PT, Rezai K, Rogers M, Andreasen NC,. Dual isotope brain SPECT imaging for monitoring cognitive activation: Initial studies in humans. *Nuc Med Comm* 1993. 14:391-6.
32. Ivanovic M, Weber DA, Loncaric S, Franceschi D. Feasibility of dual radionuclide brain imaging with I-123 and Tc-99m. *Medical Physics* 1994. 21(5):667-74.
33. Brinkmann BH, O'Brien TJ, Dresner MA, Lagerlund TD, Sharbrough FW, Robb RA. Scalp-recorded EEG Localization in MRI Volume Data. *Brain Topography* 10(4):245-253.